Comparison of RF-EM, RMT and SP measurements on a karstic terrain in the Jura mountains (Switzerland)

Frank Bosch[1], Marcus Gurk[2]

[1] Centre D'Hydrogéologie, Université de Neuchâtel, Switzerland, Frank.Bosch@unine.ch
[2] Groupe de Géomagnétisme, Institut de Géologie, Université de Neuchâtel, Switzerland, Marcus.Gurk@unine.ch

1 Introduction

The Centre of Hydrogeology Neuchâtel (CHYN) investigates and monitors karst aquifers, which are highly vulnerable to contamination. Knowledge of permeability distribution in carbonate aquifers is a fundamental condition for the understanding of water filtration processes. Permeability in fractured and karstified aquifers is essentially connected to density, orientation and opening of fractures/ conduits (Fig. 1). Extensive mapping of those fractures with direct methods is not possible when i. e. Quaternary deposits cover these structures. Additionally, direct surface observations can not provide information on the fracture distribution at greater depths. For the last 20 years several geophysical methods have been developed at the Centre of Hydrogeology Neuchâtel in order to locate the buried permeable fracture zones (depth range: 10-100 m) with "easy to handle" field equipment providing the possibility of mapping extensive areas (Bosch *et al.* 1999; Stiefelhagen 1998). The research mainly focuses on the development of electromagnetic (EM) methods (Radiomagneto-telluric = RMT; Radio Frequency-Electromagnetics = RF-EM) because they provide precise and fast measurements at a local scale.

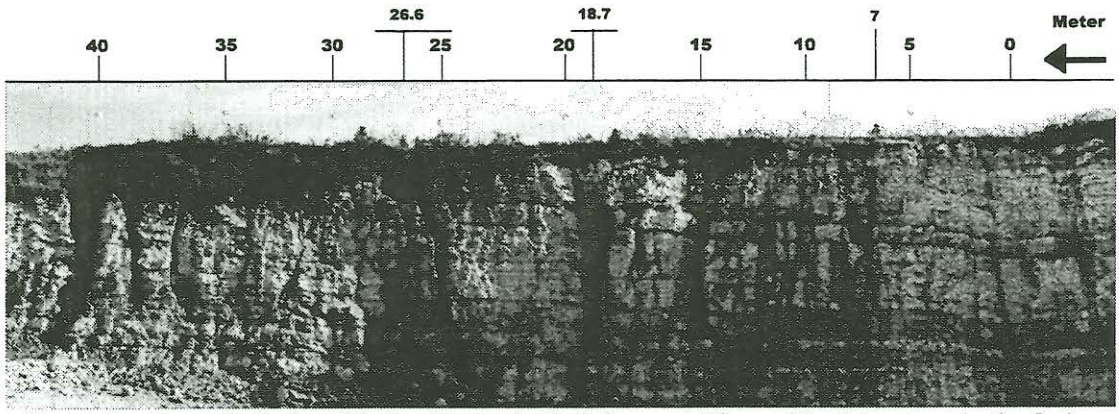

Figure 1: Example for karstified and tectonically influenced Kimmeridge Limestone in the Swiss Table Jura (Quarry of Les Breuleux, Cant. Jura, Switzerland)

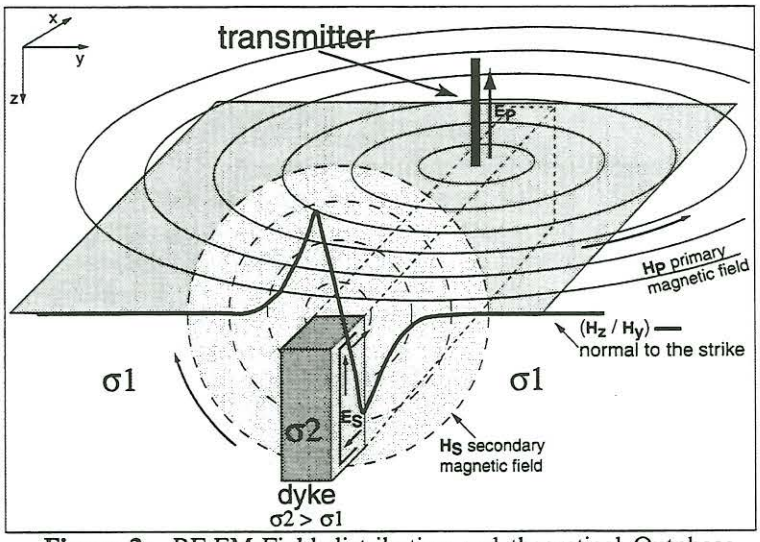

Figure 2: RF-EM-Field distribution and theoretical Outphase (Hz/ Hy) curve (after Wannamaker et al. 1985) for a thin, vertical low resistivity structure in the case of E-polarisation (redrawn after Turberg & Müller 1992).

In this case study we compare results from these EM methods, sensitive to the electric properties of the ground, with high resolution self-potential (SP) measurements. On karst, we suppose self-potential

anomalies to be generated by various effects such as physiochemical processes, streaming potentials and water-table elevation. Among these we confine ourselves on SP anomalies caused by physiochemical processes that allows detecting clay deposits in fractured zones.

2 Radio Frequency (RF) method

The RF method uses terrestrial radio transmitters in the frequency range from 15-300 kHz (Very Low Frequency=VLF up to Low Frequency=LF). The transmitters are located at several positions around the world and are used for navigation, submarine communication, time signals or public radio transmissions. The emitted EM field penetrates into the ground and induces a secondary EM field related on the electrical conductivity properties of the ground. Depth penetration is depending on the chosen frequency (Skin Effect). EM field distributions are schematically shown in Fig. 2 for the case of E-polarisation and Cartesian co-ordinates.

2.1 Radiomagnetotellurics (RMT)

The RMT method uses a linear relation between magnetic and electric field component. It measures the resultant local horizontal magnetic field component H_{Ry} with an induction coil and the secondary horizontal electrical field component by the voltage drop between two electrodes placed into the ground. Assuming E-polarisation, the *apparent resistivity* ρ_a is given by:

$$\rho_a = \frac{1}{\omega\mu}\left|\frac{E_{Sx}}{H_{Ry}}\right|^2 \qquad \text{(Cagniard 1953; Tikhonov 1950)}$$

with *transmitter frequency* $f = (\omega/ 2\pi)$ and *magnetic permeability* μ.

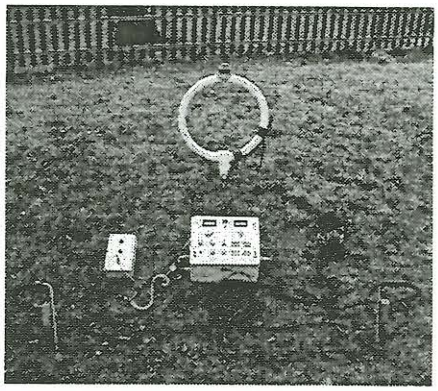

Figure 3: CHYN's RMT equipment (12-240 kHz).

CHYN's RMT equipment (Fig. 3) works in the frequency range from 12-240 kHz. Provided that μ=1, the apparatus directly delivers values of ρ_a and its *phase* φ given in Ωm and degree. This enables the application of magnetotelluric inversion schemes published by Smith, Fisher and Wu (Fischer *et al.* 1981; Smith & Booker 1991; Wu *et al.* 1993).

2.2 Radiofrequency-Electromagnetics

The RF-EM method measures the horizontal and vertical component of the *resultant local magnetic field* $\mathbf{H_R}$ with two orthogonal induction coils. Due to far-field conditions and regarding, that *primary magnetic field* $\mathbf{H_P}$ << *secondary magnetic field* $\mathbf{H_S}$ (Parasnis 1986), the measured horizontal magnetic field component can be assumed as *primary magnetic field* $\mathbf{H_P}$, where the vertical component of $\mathbf{H_R}$ is only generated by the *secondary magnetic field* $\mathbf{H_S}$.

CHYN's manual RF-EM equipment (Fig. 4) measures continuously in the frequency range of 15-300 kHz with a sample frequency of 1Hz or 4Hz. *In-phase* of (Hz/ Hy) and *Out-of-phase* of (Hz/ Hy) in (%) are written to a datalogger. Results reflect resistivity contrasts.

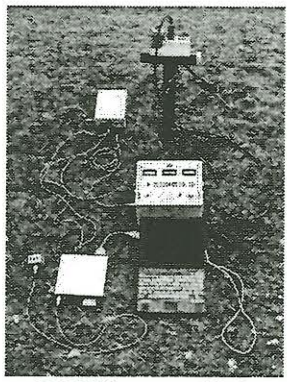

Figure 4: CHYN's manual RF-EM (15-300 kHz)

3 Selfpotential

The SP method measures the natural electric potential of the ground in mV caused by various effects (shale potential, water-table elevation, liquid junction potential, streaming potential, mineralization potential). Hence, the self-potential method can be applied for the investigation of fractured zones in limestone

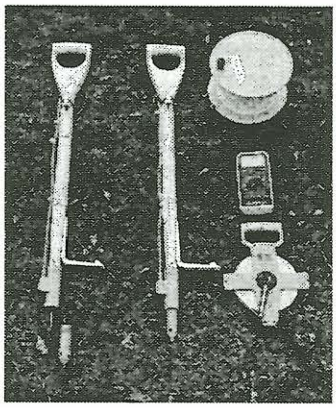

Figure 5: Selfpotential equipment "Type Münster"

filled with clay, which represent high permeability zones. For hydrogeological and hydrothermal demands, the self-potential caused by the streaming potential in porous media plays an important role and can be used to characterise the aquifer (Ishido & Pritchett 1999; Michel & Zlotnicki 1998; Revil *et al.* 1999a; Revil *et al.* 1999b).
The "Type Münster" equipment (Fig. 5) consists of saturated Cu-CuSO4 electrodes arranged on a spade stick

4 Survey Area

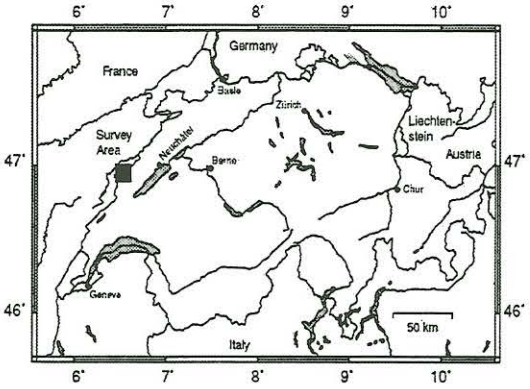

Figure 6: Map of Switzerland with survey area location

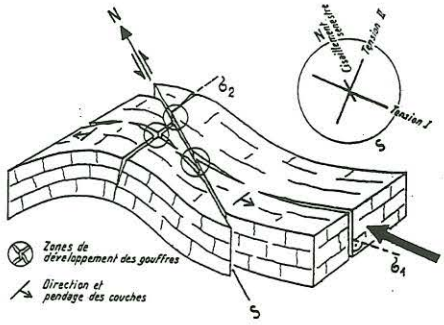

Figure 7: *Main karstification orientations in the folded Swiss Jura*: left shearing = N0°-N10°, σ_1 = N130°- N150°, σ_2 = N40°- N50° (after Müller, 1981)

The survey has been carried out over the cave of Chez-Le-Brandt near to France in the folded limestones of the Swiss Jura Mountains, canton Neuchâtel (Fig. 6). In this area Mesozoic limestone and marls crop out, covered by thin Quarternary deposits. The cave is developed in direction of about N140° in karstified limestone of the upper Sequanian/ Argovian (Fig.8) with a length of ca. 260 m. A marl layer of this sequence allowed the development of a small subterranean river. Tectonic features like faults are visible inside the cave. Another cave with an entrance in a doline has recently been detected in the centre of the profile-mesh (Fig.9, white cross). The new cave (a vertical shaft with a chamber in ca. 12 m depth) lies exactly at the position of a RF-EM anomaly measured before the cave has been discovered (profile 43.6 m, Fig 13). Inside the new cave two faults are visible with strike directions of ca. N150° & N176°. These strike directions coincide with the local stress parameters that controlled fracturing and karstification in the Swiss Folded Jura (left shearing = N0°-N10°, σ_1 = 130°-N150°, σ_2 = N40°- N50° ;Fig.7).

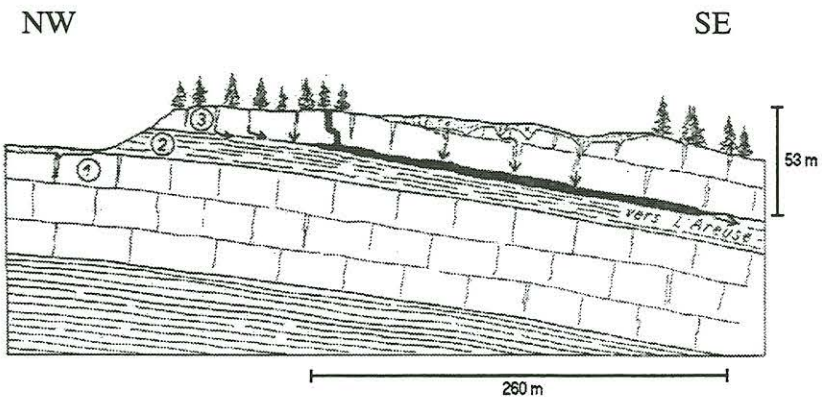

Figure 8: *Schematic geological cut of Chez le Brandt Cave area*: 1&3=karstified Sequanian/ Argovian Limestone; 2=Marl (after Müller, 1981)

5 Data

Table 1 shows the specifications for the different methods used in this case history. The main work of this survey area was focused on high resolution mapping of karst structures with RF-EM. The RMT measurements were carried out on zones of particular interest for resistivity background information. The SP method was tested as an additional tool for karst structure mapping.

For the RF-EM and RMT data it must be taken into account, that in a geological complicated environment like karstified limestone, the assumed 2D case is not likely. Therefore signal deformations due to mode mixing effects can occur as well as superposition of neighbouring anomalies. Nevertheless the transmitters were chosen due to their availability and average direction of karstic and tectonic strike

	RF-EM	RMT	SP
Transmitter-Freq./Dir.	16kHz & 19.6kHz/ N-40° 234kHz/N3°	16kHz & 19.6kHz/ N-40° 162kHz/ N100° 234kHz/N3°	-----
Sample-Frequency	4 Hz (datalogger)	5m & 10m (Profile 43.6)	1m and less
Profile Spacing	5m	in general 10m	10m

Table 1: *Data collection specifications*

directions in the Swiss Jura Mountains. Parallel profiles offer the opportunity of grouping anomalies, which belong together and indicate geological structures. This is even possible, if the shape of the measured curves is deformed.
The contour plots (Figures 9-11) present all recorded data, whereas the single profile plots (Figures 12-14) concentrate on a few profiles around the doline in the centre of the survey area.

6 Results

Generally, the contour plots of the electromagnetic results (RF-EM and RMT) enable to separate several units of different conductivity properties. In particular, the RF-EM anomalies I & II, as

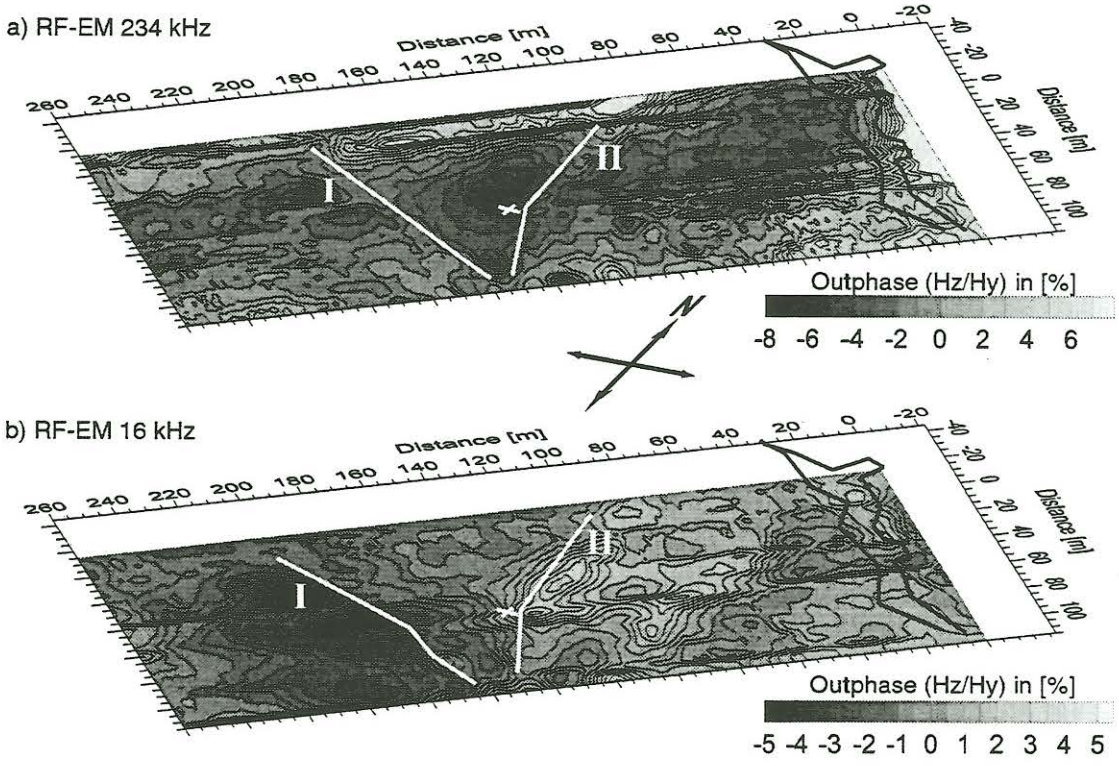

Figure 9: *Contour maps of RF-EM Data with Chez-le-Brandt cave position after speleo map.* White lines indicate two important anomalies dedicated from single profiles analysis. White cross = position of doline with entrance of new detected cave.

obtained from single profile analysis, have been graphically emphasised in the contour maps with white lines (Fig.9). Anomaly I and II are also visible in the RMT data (Fig. 10). They are thought to represent the limits of a block with slightly higher apparent resistivities (~200 Ωm) compared to the surrounding

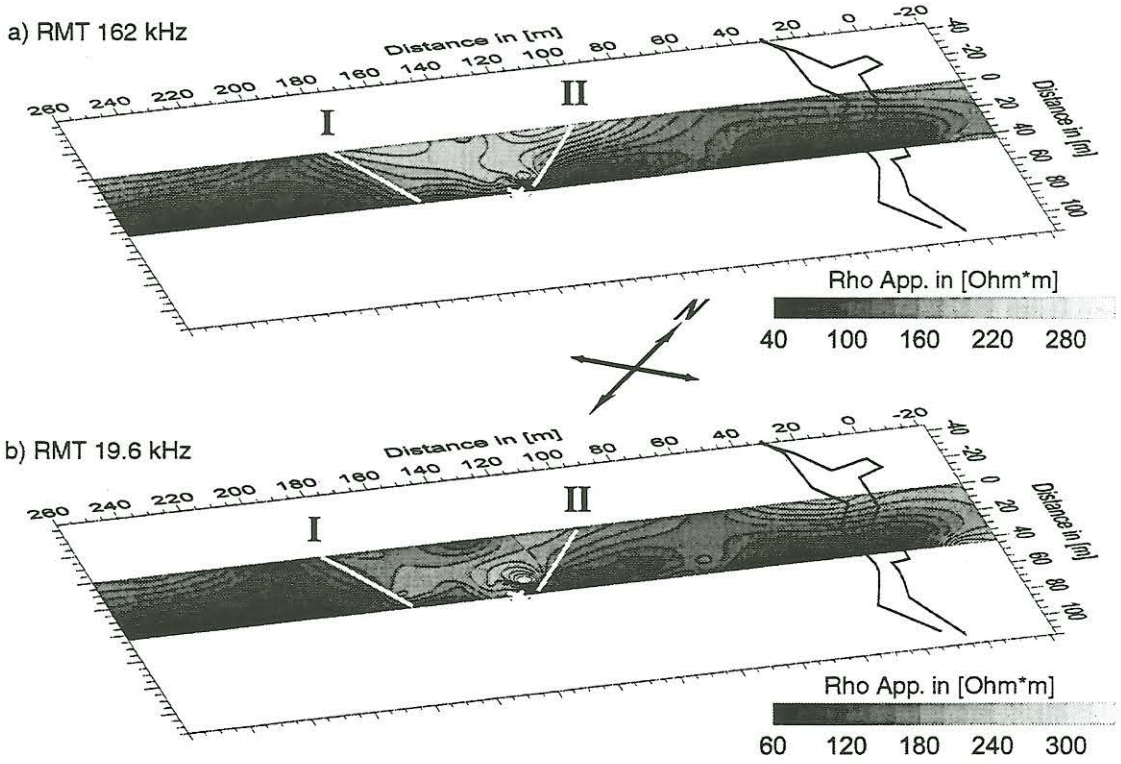

Figure 10: *Contour maps of RMT data.*

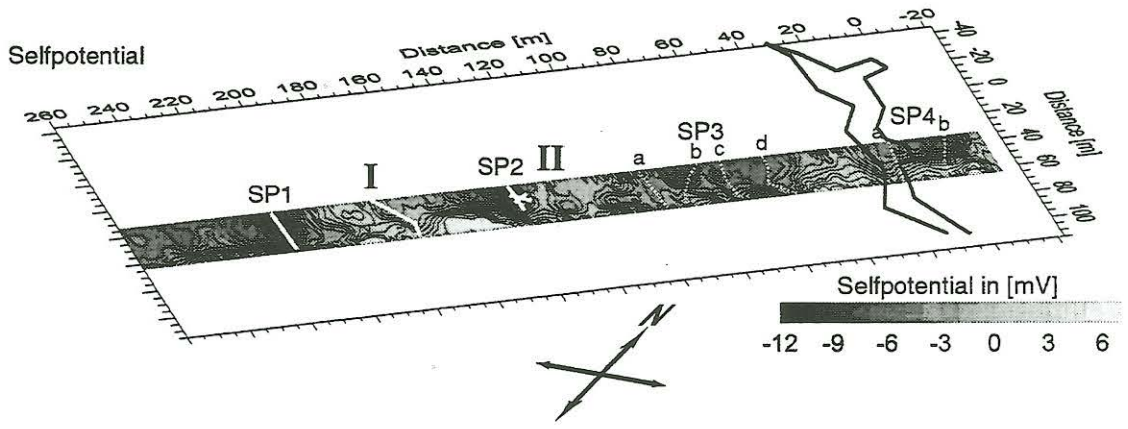

Figure 11: *Contour map of SP data.*

(~90 Ωm). The block between I and II might be interpreted as an uplifted unit due to tectonic activities (push of σ_1). The strike directions of I (~N120°) and II (~N175°, respectively south of doline ~N128°) follow the main karstification directions in the Swiss Jura Mountain as mentioned above. In particular, the strike direction of anomaly II is consistent with the two faults visible inside the new cave (white cross).

Regarding the single profiles (Figures. 13) on both sides of the "200 Ωm block", the RF-EM data show an almost equidistant series of smaller anomalies. They might be interpreted as second order fractures of anomaly I & II.

Comparing VLF and LF range, the apparent resistivities and phases in the centre of the survey area ("P33.6" & "P43.6") obtained with the RMT method show similar values. The apparent resistivity ρ_a varies between 80 Ωm and 300 Ωm and the phase φ is about 42° indicating a good conductor in the subsurface (Fig.12 & 13) followed by a more resistive halfspace. The conductor is likely formed by the low resistive marl layers embedded in the Sequanien/ Argovien limestone sequence. The following more resistive half-space is presumably caused by the decreasing degree of karstification and intrusion

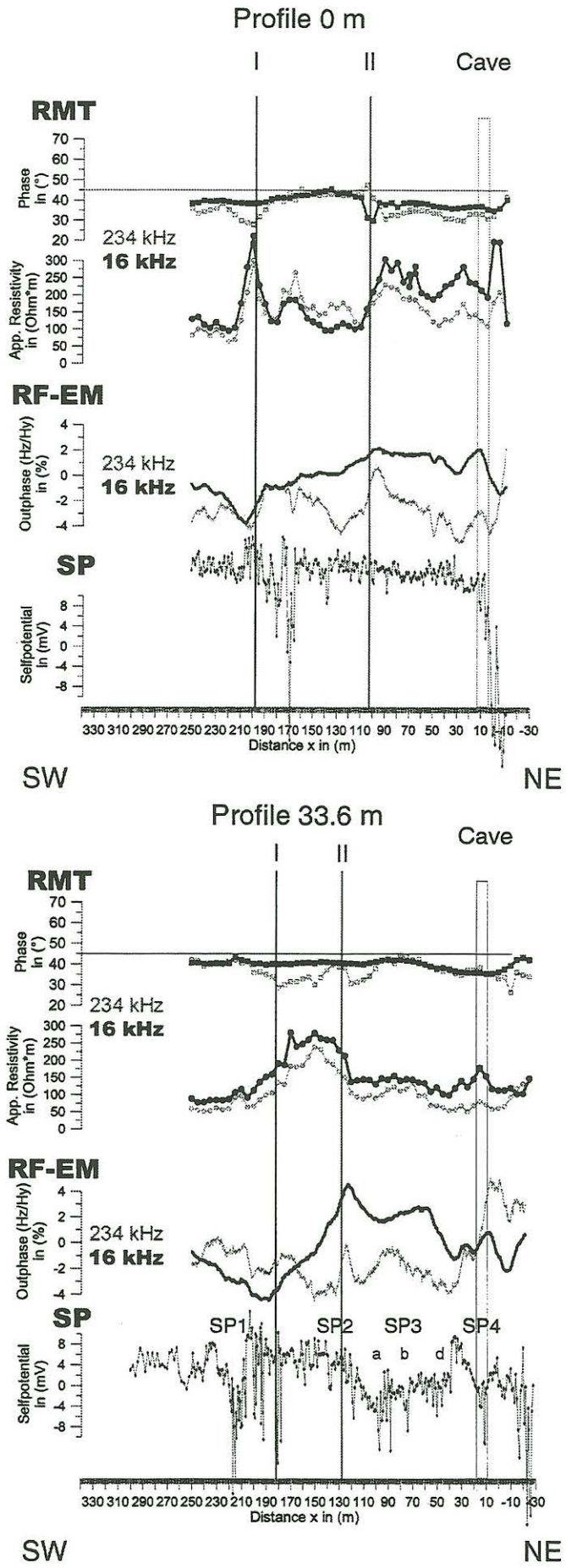

Figure 12: *Single Profile Data "Profiles 0 m & 33.6 m".*

of Quarternary deposits into the fractures. An inversion of the RMT data to model the subsurface structure has not been done yet.

In contrast to the centred RMT profiles, the profile "P0" features more lateral changes in apparent resistivity and phase (Fig. 12). One of the most striking features of this line is the maximum in resistivity at ca. 200 m. Together with the decrease of the phase it may indicate a cavity. In fact, this resistivity maximum is suited a few meter aside of RF-EM anomaly I, which is likely to indicate a fault providing a cave development.

The data content can be checked in-situ with the locations of the "Cave of Chez le Brandt" and the small cave in the centre of the survey area. And in fact, the small cave is situated at a position where the RF-EM out-of-phase anomaly I changes its strike direction and where the out-of-phase amplitude reaches maximum values. Moreover, the RMT data feature with a slight increase of apparent resistivity and a slight decrease of phase.

The RF-EM and particular the RMT data (contour plot) do not show the position of the "Cave of Chez le Brandt" very clearly. Unfortunately, the RF-EM data were disturbed by a metallic fence at the right end of the survey area. The single profiles of Figures 12 to 14 have been repeated after removing this fence. On some profiles, we find anomalies directly at the supposed position of the cave as given by a speleological map (P33.6 & P43.6). On the other profiles, data anomalies and cave positions are not coherent. Either the map is incorrect or the anomalies do not show a cave itself. In the latter case, the anomalies indicate only geological features providing cave development due to fast water flow, such as fault zones and filled fractures.

Provided that SP anomalies are generated by clay deposits in fractures, the anomaly pattern confirms the results of the EM methods and gives even additional information. From SW to NE, the SP data show in all profiles a zone of low SP variations. With the beginning of SP1, the data are

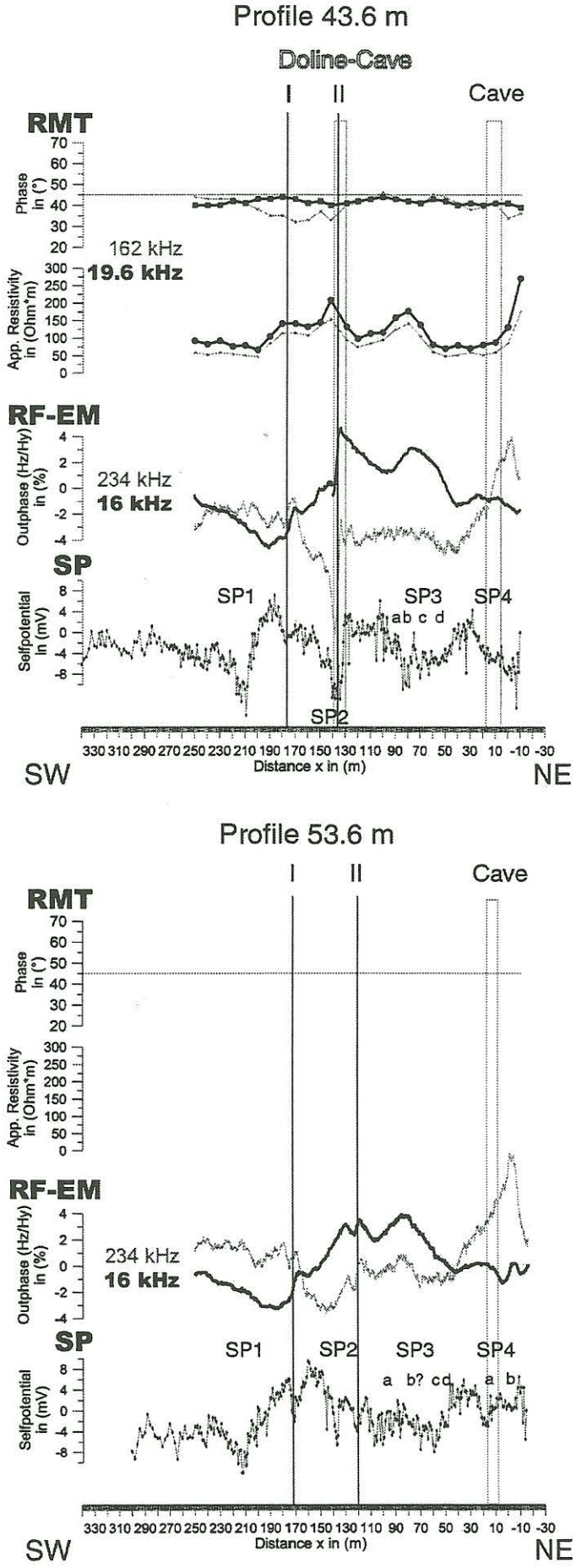

Figure 13: *Single Profile Data "Profiles 43.6 m & 63.6 m".*

characterised by an equidistantly repeating series of anomalies (SP2-SP4), where SP3 and SP4 can be subdivided into smaller anomalies. In this part, the general variation pattern is overprinted by local variations in the fracture distribution. Obviously, the SP technique is sensitive to all the characteristic features of a karstic terrain like block structures separated by more fractured zones and strong spatial variation of fracture distribution. For example, the strong anomaly "SP1" seems to be connected with several small RF-EM anomalies in the LF range. This particular RF-EM anomaly pattern could indicate several fractures at shallow depths. The SP method may indicate this part of the profile as a permeable zone in general.

Some SP anomalies shown in this study may also be created by an electrokinetical effect when ground water moves through a porous medium. The possibilities of waterflow description provided by the SP method is recently discussed (Patella 1997; Sailhac *et al.* 2000) and make the use of this method on fractured hardrock very interesting for the future. Compared to the continuously measuring RF-EM, SP suffers from slow profiling, but is still cheap and relative fast compared to other methods.

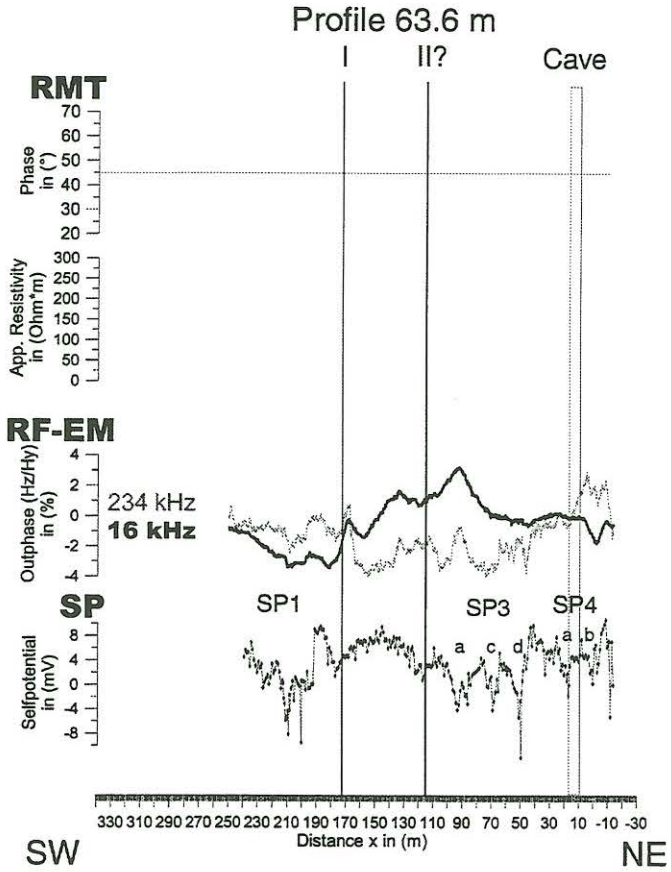

Figure 14: *Single Profile Data "Profile 63.6 m".*

7. References

Bosch, F.P., Szalai, S., Turberg, P. & Müller, I. [1999] Continuously recording radio-frequency electromagnetic (RF-EM) method (15-300 kHz) without ground contact: A powerful tool for groundwater vulnerability mapping in fissured rocks (Em4). *Proceed. of the 5th meeting of the Environmental and Engeneering Geophysical Society European Section*, Budapest 6 - 9 September 1999, Hungary, Environmental and Engeneering Geophysical Society European section.

Cagniard, L. [1953] Basic theory of the magnetotelluric method of geophysical prospecting. *Geophysics* **18**, 605-635.

Fischer, G., Schnegg, P.A., Peguiron, M. & Le Quang, B.V. [1981] An analytic one-dimensional magnetotelluric inversion scheme. *Geophysical Journal of the Royal Astronomical Society* **67**, 257-278.

Ishido, T. & Pritchett, J.W. [1999] Numerical simulation of elektrokinetic potentials associated with subsurface waterflow. *Journal of Geophysical Research* **104**(B7), 15247-15259.

Michel, S. & Zlotnicki, J. [1998] Self-Potential and magnetic surveying of la Fournaise volcano (Réunion Island): Correlation with faulting, fluid circulation and erruption. *Journal of Geophysical Research* **103**, 17845-17857.

Müller, I. [1981] La grotte de "Chez le Brandt" (Jura Neuchâtelois, Coord; 526 425/ 199 000). Essai de synthèse des donnees géologiques et hydroéologiques. *Cavernes (Neuchâtel)* **25**(1), 8-14.

Parasnis, D.S. [1986] *Principles of applied geophysics.*

Patella, D. [1997] Introduction to ground surface self-potential tomography. *Geophysical Prospecting* **45**, 653-681.

Revil, A., Pezard, P.A. & al., e. [1999a] Streaming potential in porous media, 1: Theory of the zeta potential. *Journal of Geophysical Research* **104**(B9), 20021-20031.

Revil, A., Schwaeger, H. & al., e. [1999b] Streaming potential in porous media, 2: Theory and application to geothermal systems. *Journal of Geophysical Research* **104**(B9), 20033-20048.

Sailhac, P., Marquis, G. & Aubert, M. [2000] A wavelet based technique applied to characterise subsurface fluid flow from SP data. *Proceed. of the 6th Meeting Environmental and Engeneering Geophysics - Explore Tomorrows Fundaments - Sept. 3-7 2000*, Bochum, Germany, EEGS-ES.

Smith, J.T. & Booker, J.R. [1991] Rapid Inversion of two- and three-dimensional magnetotelluric data. *J. Geophys. Res.* **96**, 3905-3922.

Stiefelhagen, W. [1998] Radio Frequency Electromagnetics (RF-EM): Kontinuierlich messendes Breitband-VLF, erweitert auf hydrogeologische Problemstellungen. *PhD thesis*, Centre of Hydrogeology, University of Neuchâtel, Neuchâtel, Switzerland, 243 pp.

Tikhonov, A.N. [1950] On determining the electric properties of deep layers of the earth's crust. *Proc (Doklady) Acad. Sci. USSR* **83-2**.

Turberg, P. & Müller, I. [1992] La méthode inductive VLF-EM pour la prospection hydrogéologique en continu du milieu fissuré. *Annales Scientifique de l' Université de Besancon, Mémoire hors série* **11**, 207-214.

Wannamaker, P.E., Stodt, J.A. & Rijo, L. [1985] PW2D - Finite element program for solution of magnetotelluric responses of two-dimensional earth resistivity structure, Earth Sciences Laboratory, University of Utah, Utah.

Wu, N., Booker, J.R. & Smith, J.T. [1993] Rapid two-dimensional inversion of COPROD2 Data. *J. Geomag. Geoelec.* **45**, 1073-1087.